NUMERICAL HYDRODYNAMIC STUDY ON THE EFFECTS OF BODY-CURVATURE DURING DITCHING

Jose D. Mesa, Kevin J. Maki

Dept. of Naval Architecture and Marine Engineering
University of Michigan
2600 Draper Drive, Ann Arbor, MI 48109
e-mail: jmesa@umich, kjmaki@umich.edu

Key words: ditching, forward-speed water entry, body surface curvature effects, computational fluid dynamics, volume-of-fluid method

Abstract. In this paper, we discuss the effects of the body curvature on the high-forward-speed water entry problem. The flow caused by aircraft ditching or planing craft slamming is characterized by a complex time-dependent wetness that is often coupled with the resulting structural dynamical response. The interaction of the complex body geometry and three-dimensional nature of the flow pose significant challenges for analytical solution development. The majority of the previous studies of this problem have been focused on pure vertical motion and flat-plate geometries, we focus on the effects of body surface curvature and large forward speed.

The present numerical study assumes the air-water flow to be governed by the Navier-Stokes equations of an incompressible two-phase but single-fluid medium. The volume-of-fluid method is employed to track the air-water interface.

The numerical framework is validated through the comparison with experiment of the force and pressure at distinct points on the body for plates that are either flat, concave, or convex. The simulations show that the body curvature produces a slight increase in the hydrodynamic force for the case of a concave plate and a reduction in force for the convex plate. An underprediction of the highly localized maximum pressure is observed between the numerical and experimental results, suggesting that a higher mesh resolution is required to fully resolve this feature. Finally, the numerical results are used to provide data for the air-water interface profile and the pressure distribution on the entire plate.

1 INTRODUCTION

The design and certification process of elastic structures that enter the water at high horizontal velocity requires the understanding of complex hydrodynamic phenomena. In the aeronautical industry, the primary concern relates to the emergency landing of an aircraft in water, referred to as ditching. A related physical process is known in naval architecture as planning-

craft slamming, where a hull experiences a violent impact on the water when traveling with large forward speed. The impact of the body develops large hydrodynamic loading that can lead to structural failure. Thus accurate prediction of the force and pressure distribution is an essential for the design and certification of aircraft and planning craft structures.

The analysis of water entry problems is challenging because air-water interface topology is complicated with a wide range of length scales (*i.e.* highly localized large surface curvature), time-dependent wetness that strongly influences the maximum value of pressure and determines the force magnitude, and large fluid density relative to the effective density of structures. The last factor requires a coupled fluid-structure interaction (FSI) analysis, and although the FSI aspect of flat-plate ditching has been studied intensely for the flat problem, the present work examines only the hydrodynamical aspects of ditching of curved surfaces.

Today the design and certification of aircraft and planning boat structures involves experimental testing and approaches based on two-dimensional hydrodynamical theory. The primary challenge in experimental campaigns is to difficulty in properly scaling for all physical process as mentioned in [1]. Furthermore, experimental testing is expensive since a specialized facility and a model is required for each structure. In the majority of theoretical approaches, the salient feature of the water entry problem such as three-dimensional effects and hydroelastic coupling is neglected [8]. Therefore, it is of interest to develop and validate high-fidelity numerical tools capable of capturing all the salient features of the water entry problem.

This numerical study aims to validate a high-fidelity numerical framework for curve bodies under high-velocity water entry problems with the experimental data presented in [6] and [5]. The successful validation of the FSI framework with high horizontal velocity for the flat-plate ditching experiments in several impact conditions is presented in [9]. While the majority of the studies of this problem have been focused on pure vertical motion and flat-plate geometries such as in [2] and [3], we focus on the effects of body surface curvature and large forward speed on the ditching hydrodynamics.

2 Numerical Framework

A detailed description of the numerical tightly-coupled fluid-structure interaction framework is found in [9]. For clarity, a brief discussion of the method fluid domain solver is presented since the structural response is not part of the scope for the current study.

The fluid domain solution is determined using computational fluid dynamics (CFD) with the volume-of-fluid (VoF) approach. The Navier-Stokes equations govern the fluid solution considering an incompressible flow of a two-phase viscous-fluid system. The finite-volume discretization combined with Arbitrary Lagrangian-Eulerian (ALE) method allows for moving and deforming fluid meshes. In this study, the ALE approach is used to rigidly move the fluid mesh. The VoF approach is suitable for complex geometries and can accurately capture the nonlinear air-water interface that develops during the ditching problem. Mainly, VoF can resolve the thin jet root, the high local pressure, the pile-up of water in front of the structure, and the three-dimensional

effects, all subject to sufficient grid resolution.

VoF is used with the Navier-Stokes equations to combine the properties of fluids (air and water) into one single continuous fluid using the volume fraction variable α. The volume fraction variable α can have any value between 0 and 1, where a value of 0 represents air, and a value of 1 represents water. Values of α between 0 and 1 represent the interface between the two fluids. The combination of VoF and the Navier-Stokes equations are shown in Equations 1 through 5.

$$\nabla \cdot \vec{u} = 0 \tag{1}$$

$$\frac{\partial \rho \vec{u}}{\partial t} + \nabla \cdot \rho \vec{u}\vec{u} = -\nabla \bar{p} + \nabla \cdot \left[\mu \left(\nabla \vec{u} + \nabla \vec{u}^T\right)\right] + \rho \vec{g} \tag{2}$$

where $\vec{u}$ is the fluid velocity, ρ is the fluid density, μ the fluid viscosity, $\bar{p}$ the fluid pressure and $\vec{g}$ the gravitational acceleration. The combination of the Navier-Stokes equations with the volume of fraction α is as follows:

$$\rho(\vec{x}, t) = \rho_{\text{water}} \alpha(\vec{x}, t) + \rho_{\text{air}}(1 - \alpha(\vec{x}, t)) \tag{3}$$

$$\mu(\vec{x}, t) = \mu_{\text{water}} \alpha(\vec{x}, t) + \mu_{\text{air}}(1 - \alpha(\vec{x}, t)) \tag{4}$$

$$\frac{\partial \alpha}{\partial t} + \nabla \cdot (\alpha \vec{u}) + \nabla \cdot (\alpha(1 - \alpha)\vec{u_r}) = 0 \tag{5}$$

The flow solver used in this work is based on the OpenFOAM CFD library, see [9] for additional details.

3 Experimental Ditching Tests and Numerical Setup

3.1 Experimental Validation Data

As previously mentioned, the understanding of the fundamental physics of high-speed water entry impact is essential for the design and certification process of complex aeronautical and marine structures. A pioneering study of high-forward-speed impact can be found in [11]. The maximum velocity during these tests was limited to 30 m/s, and the velocity during impact reduces significantly due to the small mass of the test apparatus relative to the hydrodynamic force. The data set provided in [11] provides an insight into the physical phenomena, but due to limited resolution and accuracy in measurements, the data set is not directly used for numerical tool validation.

A similar and extensive flat-plate ditching experimental campaign was carried out in [4]. Among the major improvements in [4] are use of advanced field measurement technologies, and the significantly larger mass of the system which reduces the deceleration of the test specimen

during the impact phase of the body trajectory. Also, facility uncertainty analysis performed in [7] to provide reliability in the experimental data set used for the numerical framework validation. The experimental campaign carried out in [4] for flat-plate ditching tests is further expanded in [6] and [5] to incorporate curved plates ditching tests. These latter two references form the dataset that will be used for comparison in this work.

The experimental condition simulated in this study uses shapes that are made of aluminum alloy (AL2024-T3) plate. The basic dimensions of the test specimens are 1 m long, 0.5 m wide and 15 mm thick. The radius of curvature of the surface in contact with the water is 2000 mm for both the convex and concave plates. The plate is oriented with with a 6° pitch angle, and the plate velocity is $(U, V) = (40, 1.5)$ m/s. The test condition is labeled as condition 1322 (concave plate) and 1222 (convex plate) in [5]. The experimental tests used guide rails to enforce the test-specimen body trajectory. The experiments do exhibit small reduction in velocity during the impact phase. In the numerical simulations the velocity is held constant.

3.2 Numerical Setup

Figure 1a shows the centerplane of the fluid mesh. The spatial discretization is constant in a region that extends from the leading edge of the plate through to the downstream boundary of the domain. The uniformly refined region gives a more accurate resolution of the free-surface. The computational domain has a length of three meters downstream and two meters upstream. The upstream region contains a damping relaxation zone which starts approximately 0.72 m from the leading edge of the plate and extends to the start of the domain. The damping relaxation zone ensures a calm-water-free-surface constraint in front of the plate. The total width of the numerical domain is two meters, and the plate is modeled with a symmetry plane at $y = 0$. The mesh is generated with two boundary-layer prisms with a thickness of 1 mm that are helpful to resolve the flow near the body. The numerical grid setup is based on the findings of the rectangular flat-plate ditching simulations that are presented in [10].

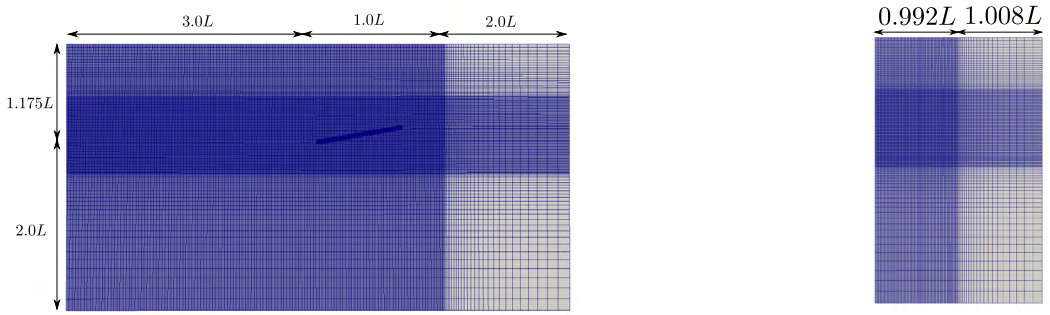

(a) Profile view of CFD mesh **(b)** Body plan view of CFD mesh

Figure 1: Fluid domain discretization for coarse grid G1 ($L = 1$ m and $\Delta x = 4$ mm).

Three grids are used to analyze resolution requirements for the different quantities of interest.

A summary of the grid resolutions is shown in Table 1. Figure 2 shows the mesh on the each of the three plates for the medium grid G2.

Table 1: CFD grid resolution

	Convex Plate		Flat Plate		Concave Plate		
Label	# of Cells	# Faces on Plate	# of Cells	# Faces on Plate	# of Cells	# Faces on Plate	Nominal Δx
G1	3,102,608	35,256	3,047,171	32,745	3,139,994	32,452	4 mm
G2	6,078,590	57,526	5,971,567	57,607	6,031,780	57,769	3 mm
G3	16,008,341	129,480	15,583,565	130,170	16,026,476	130,296	2 mm

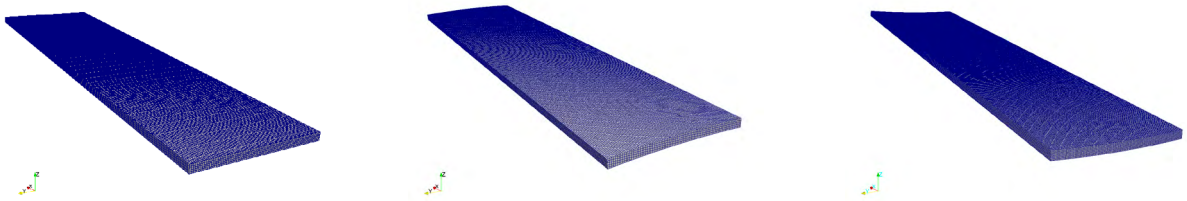

(a) Flat plate **(b)** Concave plate **(c)** Convex plate

Figure 2: Fluid mesh for G2

4 Results

4.1 Force on Plate

Figure 3 shows the vertical force on the three plates as predicted by each of the three numerical grids and the experimental measurements. Figure 3a is reprinted from [9]. Figure 3b displays the comparison between the numerical and experimental results for the concave plate. The concave ditching simulations display excellent agreement in the slope of the force and for the peak value that occurs around $t \approx 0.045$ s. The force decreases after the jet-root leaves the body, and this occurs earlier in the numerical simulations than it does in the experiment. As previously explained, the experimental test rig is freely moving along a fixed trajectory, and hence experiences a small deceleration that results in a small reduction in velocity during the impact phase. The time delay observed for the concave plate is slightly greater than the time delay observed for the flat-plate. The numerical results indicate a slightly increased force for the concave plate, which would cause a greater deceleration in the experiment and to explain the larger time shift between the numerical and experimental results. The slight increase in force could be attributed to the nature in which the water escapes from the side of the test specimen. For the concave shape the water is forced inwards towards the centerline of the body, whereas

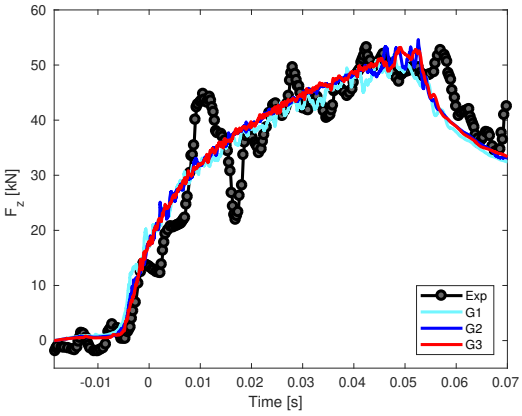

(a) Flat plate

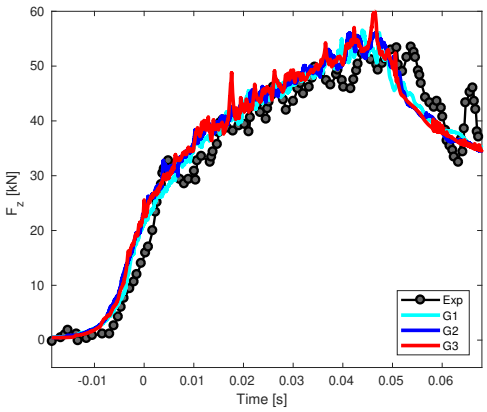

(b) Concave plate

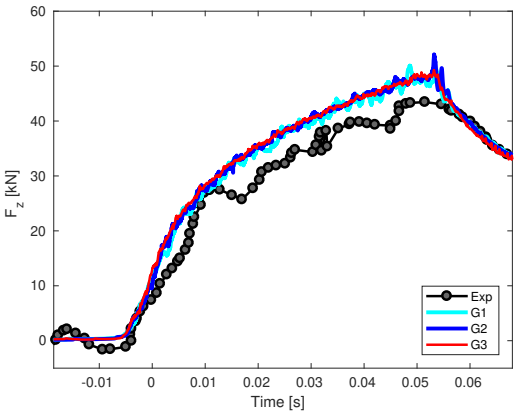

(c) Convex plate

Figure 3: Time history of the vertical force component for G1, G2, G3, and experiment (Exp) for the flat, concave and convex plates.

for the flat plate a greater amount of water can flow outwards and away from the body. Finally, it is important to note that all three grids agree strongly with each other indicating the grid resolution is sufficient for the purposes of predicting the force on the body.

Figure 3c shows the force on the convex plate. Again the agreement between the three numerical grids is very good. The comparison between the numerical and experimental results shows that the time delay due to the body deceleration is not evident, and the force in the numerical prediction is slightly larger than the experimental measurement. Overall the force for the convex plate is of smaller magnitude when compared to the concave or flat plates, and again this can be explained in the way that water can flow away from the body. This is very similar to the wedge impact problem where larger deadrise angle results in smaller forces.

In general the numerical results compare very strongly with the experimental measurements. The conclusions that can be drawn from both sources of information indicate that the force slightly increases for the concave plate when compared to a flat plate. The convex plate shows the force decreases relative to the flat plate. The small changes in force are attributed to the nature of how the flow escapes from under the body. In all three geometries the numerical results show strong agreement amongst themselves.

4.2 Pressure Probe Analysis

Figure 4 compares the local pressure coefficient time history from the experimental data and grids G1, G2 and G3. The probes are located at distances of 0.125, 0.250, 0.400, 0.600 and 0.800 m from the trailing edge along the centerline of each plate. The pressure coefficient C_p is defined as $2p/\rho(U^2+V^2)$, where p is the total pressure acting on the plate, ρ is the fluid density, U is the horizontal plate velocity, and V is the plate vertical velocity. The reference time used in Figure 4 corresponds to the time where the pressure is maximum at the first probe P4 (0.125 m).

A considerable underprediction between the experimental and numerical results can be observed for the flat and convex plate results as shown in Figure 4a and 4c respectively. The peak values of the experimental pressure for each probe exhibits significant variation for this particular ditching condition. It is noted in [4] that for pitch angles between 4° and 6°, substantial air entrapment was observed during the experiment. This complex multiphase phenomenon of spray and bubble dynamics is not accurately represented using the current grid resolution in the numerical simulations.

In contrast, the concave experimental and numerical results display a better agreement for the local pressure at locations near to the trailing and leading edges (*e.g.* 0.125, 0.250 and 0.800 m). There are larger differences between the experiments and simulations for the centrally located pressure probes which are highlighted using the green box in Figure 4b. It is believed that during impact, the first two corners of the body generate a jet-like flow that is directed towards the center of the body. When the jet flows meet on the centerline they continue to interact with each other and move together in the forward direction. This complicated flow contains spray and bubbles that are only coarsely represented in the numerical simulations.

This effect is presented in Section 4.3 and Figure 6d.

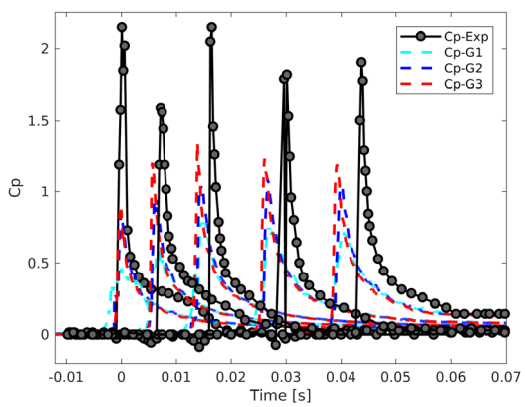

(a) Flat Plate

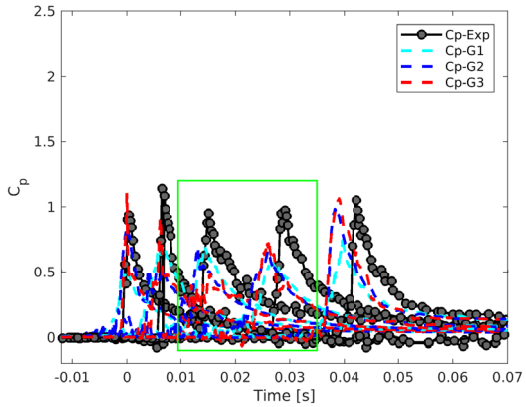

(b) Concave Plate

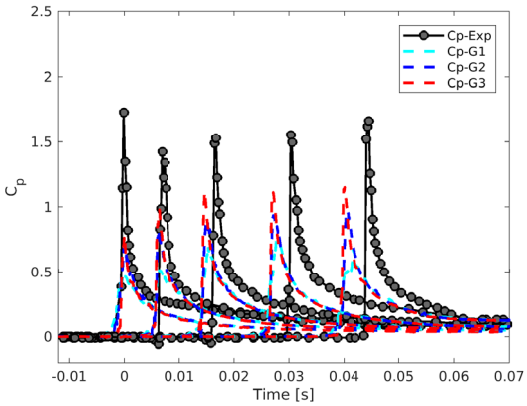

(c) Convex Plate

Figure 4: Time history of pressure coefficient C_p recorded at locations of 0.125, 0.250, 0.400, 0.600 and 0.800 m along the centerline of the flat (a), concave (b) and convex (c) plates for G1, G2, G3 grids and experiment (C_p – Exp).

In general it is observed that the effect of curvature is to reduce the maximum pressure on the plate. This effect is more pronounced for the concave plate than for the convex plate. It is very interesting to see that the effect of concavity produces a slight increase in force, but a more pronounced decrease in maximum pressure. This is believed to be due to the complex flow that develops due to the two inward-oriented jets that are produced by the edges of the concave shape that first impact the water.

The underprediction of the value of the peak in each of the numerical pressure time histories is due primarily to the lack of resolution of the numerical grid. It can be seen that as the grid is refined, the maximum value of the pressure in each probe increases and grows closer to the

experimental value. Hence the solution is not fully converged, and for the purposes of prediction of the maximum value of pressure, a finer grid yet is necessary.

4.3 Spatial Flow Field Analysis

Lastly, to provide an insight into how body curvature affects the flow during ditching, the air-water interface and pressure-profile on the plate are presented. Figure 5 displays a transverse profile of the water surface elevation η. The profile is located at a streamwise position of the plate trailing edge for plates at an instant in time when the jet root has approximately reached 0.400 m along the plate. The horizontal axis is the dimensionless transverse coordinate defined as $\xi = y/B$. Close agreement is observed for the free surface topology as the grid resolution increases for all plate geometries. The water surface elevation maximum value is highest for the flat plate and slightly reduces for the concave and convex plate respectively.

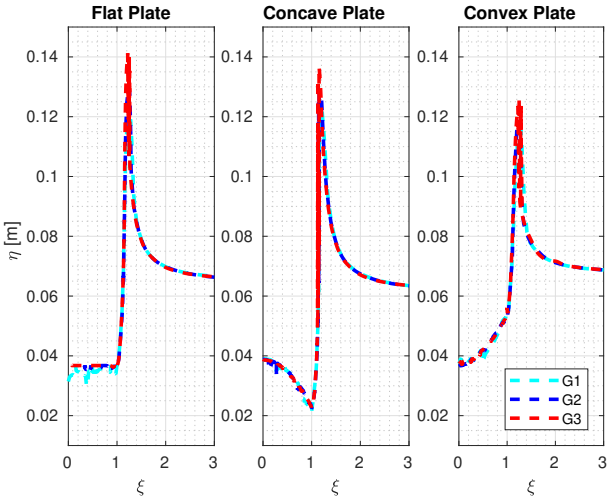

(a)

Figure 5: Water surface transverse profile.

A full three-dimensional view of the water surface is shown together with the pressure coefficient on the plate in Figure 6. The imprint of the different body shapes is clearly seen in the region where the body first impacts the water surface. For the flat plate, the initial depression in the calm water appears as a straight line behind the trailing edge of the plate. In the case of the concave and convex plates, the depression follows either a V or U behind the trailing edge of the plate. The pressure coefficient distribution for the flat plate follows a parabolic shape with a smaller curvature compared to the convex plate. In the case of the concave plate the unique feature along the center of the plate shows the interacting edge-generated jets that are discussed previously in the text with regard to the pressure probe data.

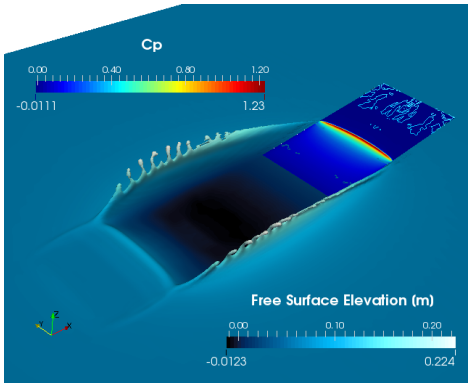

(a) Flat plate isometric view

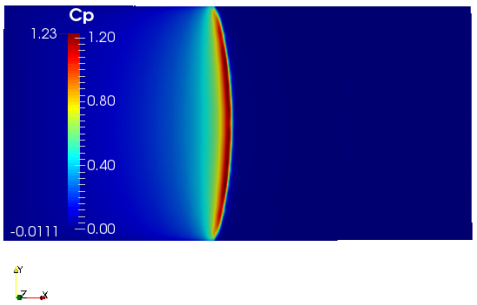

(b) Flat plate top view

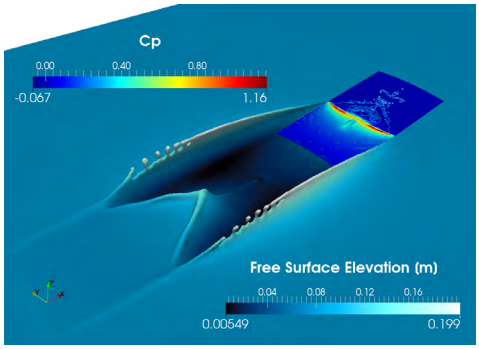

(c) Concave plate isometric view

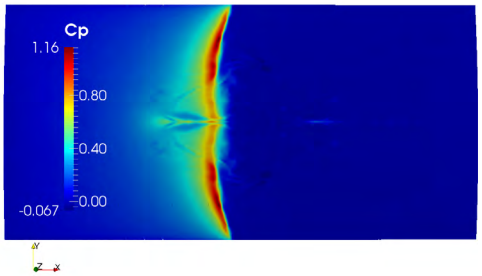

(d) Concave plate top view

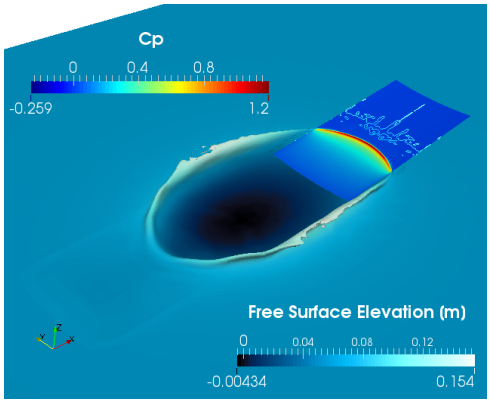

(e) Convex plate isometric view

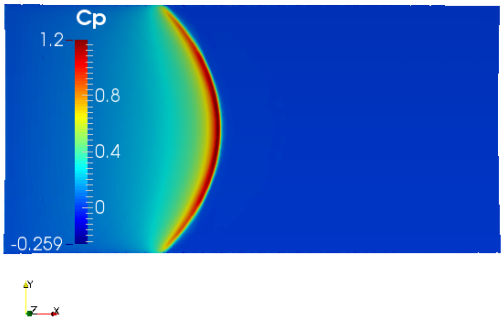

(f) Convex plate top view

Figure 6: Visualization of the water surface and pressure coefficient distribution on the plate during the time when the jet root approximately reaches 0.400 m.

5 CONCLUSIONS

In this paper the hydrodynamics of a body entering the water with high forward speed are studied with a numerical computational fluid dynamics solver. In particular the effect of body curvature is analyzed by comparing results of a concave and convex shape to those of a flat plate. Comparison with an extensive experimental campaign is used to assess the accuracy and convergence of the numerical results.

The numerical solution captures the curvature effects on the hydrodynamic force and is in strong agreement with the experimental data. For the concave plate a slight increase in force is observed, but overall the force component follows the same trend as the flat plate. On the other hand, for the convex plate a more noticeable force reduction is observed.

It is observed that the overall effect of plate curvature on the maximum pressure along centerline is to reduce the local pressure magnitude. The reduction in local pressure is more significant for the concave plate due to the complex interacting jet flow that forms with the two edges of the plate that first impact the water and generate spray and bubbles.

The numerical results demonstrate that the grids used in this work are sufficient for force prediction purposes. The maximum pressure is not fully converged, and grids with additional resolution on the body are required to more confidently predict the maximum value. The numerical results are useful to predict the full flow field including the pressure distribution on the plate and the water surface distribution.

REFERENCES

[1] H. Climent, L. Benitez, F. Rosich, F. Rueda, and N. Pentecote. Aircraft ditching numerical simulation. In *25th Int. Congress of the Aeronautical Sciences, Hamburg, Germany*, 2006.

[2] O. M. Faltinsen. The effect of hydroelasticity on ship slamming. *Philosophical Transactions of the Royal Society of London A: Mathematical, Physical and Engineering Sciences*, 355(1724):575–591, 1997.

[3] O. M. Faltinsen, J. Kvålsvold, and J. V. Aarsnes. Wave impact on a horizontal elastic plate. *Journal of Marine Science and Technology*, 2(2):87–100, 1997.

[4] A. Iafrati. Experimental investigation of the water entry of a rectangular plate at high horizontal velocity. *Journal of Fluid Mechanics*, 799:637–672, 2016.

[5] A. Iafrati. Effect of surface curvature on the hydrodynamics of water entry at high horizontal velocity. In *ASME 2018 37th International Conference on Ocean, Offshore and Arctic Engineering*, pages V009T13A034–V009T13A034. American Society of Mechanical Engineers, 2018.

[6] A. Iafrati. Effect of the body curvature on aircraft ditching hydrodynamics. In *33th IWWWFB, Guidel-Plages, France*, 2018.

[7] A. Iafrati, S. Grizzi, M. Siemann, and L. B. Montañés. High-speed ditching of a flat plate: Experimental data and uncertainty assessment. *Journal of Fluids and Structures*, 55:501–525, 2015.

[8] A. Iafrati and Korobkin. Self-similar solutions for porous/perforated wedge entry problem. In *20th IWWWFB, Longyearbyen, Norway*, 2005.

[9] J. D. Mesa. *Hydroelastic Analysis of Aluminum and Composite High-Speed Planing Craft Structures During Slamming*. PhD thesis, The University of Michigan, 2018.

[10] J. D. Mesa and K. J. Maki. Numerical investigation of rectangular flat plate slamming. In *ECCOMAS Congress 2018, Glasgow, UK*, 2018.

[11] R. F. Smiley. An experimental study of water-pressure distributions during landing and planing of a heavily loaded rectangular flate-plate model. Technical report, National Aeronautics And Space Administration Washington DC, 1951.